

## GAMMA-RAY BURST FLARES: X-RAY FLARING. II.

C. A. SWENSON<sup>1</sup>, P. W. A. ROMING<sup>2,1</sup>

*Submitted to ApJ*

### ABSTRACT

We present a catalog of 497 flaring periods found in gamma-ray burst (GRB) light curves taken from the online XRT GRB Catalogue. We analyzed 680 individual light curves using a flare detection method developed and used on our UV/optical GRB Flare Catalog. The method makes use of the Bayesian Information Criterion to analyze the residuals of fitted GRB light curves and statistically determines the optimal fit to the light curve residuals in attempt to identify any additional features. These features, which we classify as flares, are identified by iteratively adding additional ‘breaks’ to the light curve. We find evidence of flaring in 310 of the analyzed light curves. For those light curves with flares, we find an average number of  $\sim 1.5$  flares per GRB. As with the UV/optical, flaring in our sample is generally confined to the first 1000 s of the afterglow, but can be detected to beyond  $10^5$  s. Only  $\sim 50\%$  of the detected flares follow the ‘classical’ definition of  $\Delta t/t \ll 1$ , with many of the largest flares exhibiting  $\Delta t/t \sim 1$  and some exceeding this value.

*Subject headings:* gamma-ray burst: general

### 1. INTRODUCTION

The *Swift* (Gehrels et al. 2004) mission has revolutionized the study of Gamma-ray Burst (GRB) afterglows due to its rapid response time and automated GRB response algorithms. *Swift* is comprised of three instruments that work together and all contribute their unique capabilities to this the study of GRBs. The Burst Alert Telescope (BAT; Barthelmy et al. 2005) first detects the GRB and causes the satellite to perform an autonomous slew to the GRB position, generally within  $\sim 100$  seconds of the GRB trigger. The X-ray Telescope (XRT; Burrows et al. 2005b) and UV/Optical Telescope (UVOT; Roming et al. 2000, 2004, 2005) then begin an automated sequence of observations designed to localize the position of the GRB to less than an arcsecond and follow the decay of the afterglow. *Swift* has triggered on and localized an X-ray counterpart for over 700 GRBs, increasing the number of afterglow localizations by approximately an order of magnitude from the pre-*Swift* era. The rapid localizations and follow-up provided by *Swift* has resulted in several exciting new discoveries about the properties of the GRB afterglow, including the “canonical” X-ray light curve (Nousek et al. 2006), which is observed in a number of GRBs (e.g. Hill et al. 2006, Evans et al. 2009). Also discovered early in the *Swift* mission was the presence of X-ray flares in the early afterglow (e.g. Burrows et al. 2005a, Romano et al. 2006).

Flares in GRB afterglows had been seen previous to their observation by the XRT (e.g. Piro et al. 1998, 2005), but only in three X-ray afterglows. The XRT observations have shown that flares are seen in phases of the canonical X-ray light curve and quite common, appearing in approximately 50% of the XRT afterglows (O’Brien et al. 2006). These flares are observed as superimposed excesses deviating from the underlying light

curve.

Through the study of individual flares in GRBs 050406 (Romano et al. 2006), 050502B (Falcone et al. 2006), 050713A (Morris et al. 2007), 050724 (Campana et al. 2006) and 050904 (Cusumano et al. 2007) it has been shown that X-ray flares are observed in both long and short GRBs, appear to come from a distinctly different emission mechanism than the underlying afterglow, and can be observed out to beyond  $10^5$  seconds from the initial GRB trigger (e.g. Swenson et al. 2010). These studies also point toward a likely internal shock source for the flares, though the actual source of the flares still remains in question and may be caused by one of many different mechanisms including instabilities in the ejecta, stored electromagnetic energy or collision with the extrastellar medium (Zhang et al. 2006).

Studying large numbers of flares from several different bursts, and analyzing their bulk properties allows us to try and better constrain the physical process by which flares are created. Several previous studies have been performed on XRT light curves, analyzing groups of X-ray flares. The earliest studies by Falcone et al. (2007) and Chincarini et al. (2007) examined 33 flares in the first 110 GRBs observed by *Swift*. These studies showed that late-time internal shocks were necessary to explain the 10 of the observed flares and that some sort of central engine activity was the preferred method for a majority of the flares. Follow-up studies performed by (Chincarini et al. 2009, 2010) and (Margutti et al. 2010) showed that X-ray flaring may have some correlation with the GRB prompt emission and showed that flares evolve over time, and were likely caused by late-time internal dissipation processes.

Morris (2008) did incorporate the BAT, XRT and UVOT data for the flare sample used by Falcone et al. (2007) and Chincarini et al. (2007) and showed that whereas the afterglow could be fit by a simple absorbed power law, the SED of the flaring periods could not. (Roming et al. 2006) attempted to perform a study analyzing flares in the UV/optical but was severely limited

cswenson@astro.psu.edu

<sup>1</sup> Pennsylvania State Univ., 525 Davey Lab, University Park, PA 16802, USA

<sup>2</sup> Southwest Research Institute, 6220 Culebra Road, San Antonio, TX 78238, USA

due to the low significance of UV/optical flares compared to X-ray flares.

Realizing the need for more detected flares in the UV/optical, in our first paper (Swenson et al. 2013) we presented a catalog of flares found in the UV/optical from the collection of light curves presented in the Second *Swift* Ultraviolet/Optical Telescope GRB Afterglow Catalog, an expansion on the First *Swift* Ultraviolet/Optical Telescope GRB after Catalog (Romig et al. 2009). These flares were found using a new algorithm developed specifically for the purpose of performing a blind, systematic search for flares in GRB afterglows. This search resulted in the discovery of 119 potential flaring periods in 68 GRB afterglows, many of which were previously undetected. This study showed that flares in the UV/optical are much more common than has previously been thought.

As mentioned previously, many of the studies on X-ray flares were limited in their reach due to limitations in their data sets. Falcone et al. (2007) and Chincarini et al. (2007) were limited by the time that *Swift* had been operating, Chincarini et al. (2009) limited their data set to GRBs with redshift measurements to study the actual energetics, Chincarini et al. (2010) limited their study to only flares found within the first 1000 seconds of the GRB afterglow, and Margutti et al. (2010) used only a sample of 9 exceptionally bright X-ray flares. There has yet to be a blind, systematic search for X-ray flares that is not somehow limited in scope.

The precise nature of the GRB central engine is still largely unknown and many of the previous studies on GRB flares have indicated a likely connection between flaring and the central engine, making the study of GRB flares crucial to our understanding of GRBs. Having a complimentary X-ray catalog using the algorithm developed in Swenson et al. (2013) would address the limitations mentioned in the previous X-ray studies and allow for more stringent constraints on the origin of GRB flares through cross-correlation of the X-ray and UV/optical.

In this paper we present the results from a blind, systematic search for flares in XRT light curves. Using the method described in Swenson et al. (2013) we have constructed the most complete catalog of X-ray flares to date and provide the temporal details of each flare, including  $T_{peak}$ ,  $\Delta t/t$ , and the strength of the flare relative to the underlying light curve. In a forthcoming paper we will perform our cross-correlation analysis of this catalog and our UV/optical flare catalog.

This paper is organized as follows: In §2 we describe our data set as well as our methodology for identifying flares. We present our catalog of GRB flares observed by the XRT in §3, and discuss the implications drawn from the catalog in §4.

## 2. METHODOLOGY

For the purposes of this study we will use the publicly available XRT light curves from the online Swift-XRT GRB Catalogue (Evans et al. 2007, 2009). We downloaded the light curves for the time period covering January 2005 through December 2012, inclusive, as well as the best fit parameters for each burst. We calculated the light curve residuals using the best fit parameters and perform our flare finding analysis on these residuals.

Our flare finding analysis follows the same basic

methodology set forth in Swenson et al. (2013). We processed the calculated residuals using the breakpoints analysis function (Zeileis et al. 2003) within the publicly available R (R Core Team 2013) package `structchange` (Zeileis et al. 2002). The breakpoints analysis determines the optimal number of ‘breakpoints’ that are required to best explain any features that may remain in the residuals of the GRB light curve. This is done by simultaneously minimizing both the residual sum of squares (RSS) and the Bayesian Information Criterion (BIC; Schwarz 1978) over several iterative fits to the light curve. For the purposes of our analysis we used the guidelines provided by Kass & Raftery (1995) and require  $BIC_i - BIC_{min} > 6$  as the criteria for determining the preferred fit to the light curve residuals.

We performed 10,000 Monte Carlo iterations for each GRB light curve, each time varying the datapoints to account for measurement error and then determining the optimal number of breakpoints and grouping those breakpoints into potential flares. For each potential flare we identify the following parameters:  $T_{start}$ ,  $T_{peak}$  and  $T_{stop}$ , the start, peak and end times of each flare, respectively, each nominally associated with an individually identified breakpoint. Due to the higher density of data points, and therefore timing resolution, our determinations of  $T_{start}$  and  $T_{stop}$  will be more precise than for the UV/optical flares, but we will continue to refer to them as ‘limits’ because there are still instances of poor timing resolution and gaps in the data that prevent us from determining a more accurate breakpoint. We calculated  $\Delta t/t$ , defined as  $(T_{stop} - T_{start})/T_{peak}$ , and the peak flux ratio using the measured flux at  $T_{peak}$  and an interpolation of the flux of the underlying light curve at the same time. We also provide a confidence measure, which we define as the fractional number of times that a particular flare was recovered during the 10,000 simulations.

A few minor changes in the actual processing of the data were required, as opposed to the UV/optical dataset. Due to the much higher density of data points available in many of the X-ray light curves, as opposed to the relatively sparsely sampled UV/optical light curves, we were forced to limit the number of potential breakpoints identified to 75 per light curve. By default the analysis iteratively adds additional breakpoints between ever data point in the light curve, beginning with the strongest (i.e. most likely) breakpoint. This process is computationally intensive and adding an arbitrarily large number of additional breakpoints increases the processing time exponentially. By limiting the number of breakpoints to 75 we are allowing for a minimum of 25 individual flares per light curve. Our results presented in this paper show that no burst had more than nine individual flares identified, so the truncation of the analysis had no effect on the end results.

Additionally, due to the number of data points contained in some of the brightest X-ray light curves, the process of iteratively fitting every data point requires a large number of CPU cycles and completing the normal 10,000 Monte Carlo iterations would have required several years of computational time. In those cases we limited the number of iterations to 1,000 Monte Carlo simulations and report our confidence measure as the fraction of times the flare was recovered for those 1,000 simulations.

### 3. RESULTS

Here we present the results of our analysis of the 680 XRT GRB light curves taken from the online Swift-XRT GRB Catalogue (Evans et al. 2007, 2009) spanning January 2005 to December 2012, inclusive. We detect 497 unique potential flaring periods, for which we can distinguish start and stop times, detected in 324 different light curves. A number of these identified flares are actually multiple superimposed flares contained within a shared ‘flaring period’. Because of the high density of data points in the X-ray light curves, we are able to resolve periods of multiple overlapping flares. Due to the overlapping, we can not uniquely identify the start or stop of the individual flares within the larger ‘flaring period’. We are limited to identifying only the start and stop times of the entire period containing the overlapping flares. For the sake of simplicity and completeness we will include these flaring periods in our analysis and simply refer to these flaring periods as ‘flares’. Table 1 provides the following information for each potential flare: (1) GRB Name, (2) the flare peak time, defined as the data point most often identified as the flare peak during the Monte Carlo simulations, as well as limits on (3)  $T_{start}$  and (4)  $T_{stop}$ , defined as the last and first data points, respectively that are well fit by the underlying light curve. (5) a limit on  $\Delta t/t$  based on the peak time,  $T_{start}$  and  $T_{stop}$ , and (6) the ratio of the peak flux during the flaring period, relative to the flux of the underlying light curve at the same time, using the observed flux at the flare peak time and an interpolation of the flux of the underlying light curve. The flux ratio is normalized using the flux of the underlying light curve to allow for direct comparison of each flare across all light curves. Finally, (7) the confidence measure of the detected flare indicating the fractional number of times the flare was recovered during the 10,000 Monte Carlo simulations. We have noted the overlapping ‘flaring periods’ with an ‘\*’ next to the GRB name in Table 1.

### 4. DISCUSSION

Our analysis shows that at least 47% of the analyzed XRT light curves contain possible flaring episodes. This percentage is very similar to previous studies (e.g. O’Brien et al. 2006; Chincarini et al. 2010), in spite of our detection of a significantly larger number of total flares and specifically a larger number of small, weak flares. This may indicate that X-ray GRB afterglows comes in two varieties: those with flares and those without.

In our analysis of the bulk properties of the detected X-ray flares we have followed the same method used in Swenson et al. (2013) and divided the flares into three groups: “gold”, “silver” and “bronze”. Our comparisons to uv/optical flares will also come from our analysis found in Swenson et al. (2013).

The gold group is defined as those flares with confidence measure greater than 0.7 and  $\Delta t/t \leq 0.5$ . This group constitutes those flares which satisfy the somewhat “classical” definition of a flare in terms of duration and have a good recoverability rate. This group contains 127 flares. The silver group allows for longer flares and lower confidence, expanding the parameters to confidence measure greater than 0.6 and  $\Delta t/t \leq 1.0$ . This group con-

tains 115 flares after excluding overlap from the gold group. The remaining flares that do not qualify for either the gold or silver are grouped together in the bronze, which contains 255 flares.

Of the 323 X-ray light curves with flares, the average number of flares per GRB is  $\sim 1.5$ . Figure 1 shows the distribution of flares per GRB for the gold, silver and bronze groups, shown in black, blue, and red, respectively. GRB100728A had the most resolved flares of the analyzed bursts, with nine, and five other GRB light curves had five or more flares.

The flare peak times range from between 48 s after the trigger of GRB 110119A to over 400 ks for GRB 090902B. 82% of all detected flares peaked before 1000 s, nearly matching the percentage seen in the UV/optical light curves. We suspect that this similarity to the UV/optical flares is not coincidental and that many of these flares may be correlated, or at the very least caused by a similar mechanism that is active during the early stages of the GRB. This issue will be looked at in depth in our next paper correlating the UV/optical and X-ray flares. Figure 2 shows the distribution of  $T_{peak}$  for the three groups of flares. The grouping of  $T_{peak} \leq 1000$  s is immediately obvious in all three groups, and all three groups appear to originate from a similar parent distribution peaking between 300 s and 500 s after the trigger.

The duration of the flares, recognizing that a number of the  $T_{start}$  and  $T_{stop}$  values are only limits, vary from  $\Delta t/t$  of 0.02 to over 100 (though the extremely large values are due to observing gaps in the data). Only  $\sim 50\%$  of the flares exhibited  $\Delta t/t \leq 0.5$ , whereas this number was at least 80% for the UV/optical flares. This difference between the duration of the X-ray and UV/optical flares may be due to the UV/optical flares being generally fainter than those seen in the X-ray. If we only see the peak of the flare in the UV/optical, then our measured duration for the flare will be biased relative to the X-ray where we see more of the flare rise and decay. Figure 3 shows the distribution of  $\Delta t/t$  for the three groups of flares. Ioka et al. (2005) showed that it is difficult to achieve rapid variability, defined as  $\Delta t/t \leq 1$ , in the external shock and so an internal shock model has been favored to explain the  $\Delta t/t \ll 1$  seen in most flares. However, Figure 3 shows a significant number of possible flares that exhibit  $\Delta t/t > 1$ . For this work we are reporting all potential features detected by our flare finding algorithm, and we treat them as potential flares. It is possible, however, that a portion of our detected features, in particular those with  $\Delta t/t \geq 1$ , are due to other processes, such as the emergence of the reverse shock, and are not flares. It is also possible that these are flares caused by processes other than internal shocks. An interesting relationship between the gold, silver and bronze groups needs to be pointed out when interpreting Figure 3. There is a continuous distribution of potential flares that is spread across the three groups. We split the detected flares into three groups based on the prior understanding of flare properties, namely  $\Delta t/t \ll 1$ , and so created groups based on the combination of flare recoverability and  $\Delta t/t$ . Many of the very large and most easily identified potential flares exhibit  $\Delta t/t > 0.5$  and some  $\Delta t/t > 1.0$ . Because the flares do not meet the criteria for the gold group they spill over into the silver and bronze groups. This can be seen by the abrupt cut-

off, based on our group criterion, in the gold group at  $\Delta t/t = 0.5$  and the subsequent continuation of the distribution in the silver group between  $0.5 < \Delta t/t \leq 1.0$  and the excess tail extending into the bronze group at  $\Delta t/t > 1.0$ . These large flares comprise the majority of the silver group, with the remaining flares being distributed at  $\Delta t/t < 0.5$ . The primary distribution of the bronze flares, removing the extended tail from the gold and silver groups, can be seen at  $\Delta t/t < 1.0$  and peaking at  $\Delta t/t \sim 0.1$ .

The relative strengths of the flares ranges from a minimum flux ratio of 0.1 to a maximum of several thousand. Figure 4 shows the distribution of flare flux ratios for the three groups for values  $< 5$ . All three groups of flux ratios have long tails that extend into the tens, hundreds, and thousands for the gold, silver, and bronze groups, respectively. The flux ratios shown in Figure 4 show the distributions for those smaller, weaker flares that have previously been less studied. Unlike the UV/optical flares, which had noticeable gaps in the distributions of flux ratios, the X-ray flares show a much more continuous distribution. The silver group appears to have either a bimodal distribution with peaks at 0.6 and 1.3, or a continuous distribution that is suppressed near a flux ratio of 1.0. This same suppression also appears in the bronze distribution as a sudden dropoff at flux ratios  $> 1.0$ , rising again to a peak at 1.3. The gold group does not exhibit the suppression at flux ratio of 1.0 but is well fit by a distribution centered at  $\sim 0.8$ . Only a small number (17%) of UV/optical flares were considered to be strong flares with flux ratios  $> 2$ . By that same criteria 33% of X-ray flares are considered large, showing the relative strength of X-ray flares compared to the UV/optical flares.

## 5. CONCLUSIONS

We have analyzed 680 XRT GRB light curves from the online Swift-XRT GRB Catalogue (Evans et al. 2007, 2009) using the flare detection method introduced in Swenson et al. (2013). We detect the presence of 497 unique potential flaring periods, many of them previously unreported. We plan to perform a cross-correlation analysis of the UV/optical flares provided in Swenson et al. (2013) and the X-ray flares reported in this work. By using the multi-wavelength flare information from these two catalogs we will be able to better constrain the properties of GRB flares and better understand their origin.

We thank Eric Feigelson for his help in pointing us toward the use of the Bayesian Information Criterion. This work made use of the data supplied by the UK Swift Science Data Centre at the University of Leicester.

## REFERENCES

- Barthelmy, S. D., Barbier, L. M., Cummings, J. R., et al. 2005, *Space Science Reviews*, 120, 143  
 Burrows, D. N., Romano, P., Falcone, A., et al. 2005a, *Science*, 309, 1833

- Burrows, D. N., Hill, J. E., Nousek, J. a., et al. 2005b, *Space Science Reviews*, 120, 165  
 Campana, S., Tagliaferri, G., Lazzati, D., et al. 2006, *Astronomy and Astrophysics*, 454, 113  
 Chincarini, G., Margutti, R., Mao, J., et al. 2009, *Advances in Space Research*, 43, 1457  
 Chincarini, G., Moretti, A., Romano, P., et al. 2007, *The Astrophysical Journal*, 671, 1903  
 Chincarini, G., Mao, J., Margutti, R., et al. 2010, *Monthly Notices of the Royal Astronomical Society*, 406, 2113  
 Cusumano, G., Mangano, V., Chincarini, G., et al. 2007, *Astronomy and Astrophysics*, 462, 73  
 Evans, P. A., Beardmore, A. P., Page, K. L., et al. 2007, *Astronomy and Astrophysics*, 469, 379  
 —. 2009, *Monthly Notices of the Royal Astronomical Society*, 397, 1177  
 Falcone, A. D., Burrows, D. N., Lazzati, D., et al. 2006, *The Astrophysical Journal*, 641, 1010  
 Falcone, A. D., Morris, D., Racusin, J. L., et al. 2007, *The Astrophysical Journal*, 671, 1921  
 Gehrels, N., Chincarini, G., Giommi, P., et al. 2004, *The Astrophysical Journal*, 611, 1005  
 Hill, J. E., Morris, D. C., Sakamoto, T., et al. 2006, *The Astrophysical Journal*, 639, 303  
 Ioka, K., Kobayashi, S., & Zhang, B. 2005, *The Astrophysical Journal*, 631, 429  
 Kass, R., & Raftery, A. 1995, *Journal of the American Statistical Association*, 90, 773  
 Margutti, R., Guidorzi, C., Chincarini, G., et al. 2010, *Monthly Notices of the Royal Astronomical Society*, 406, 2149  
 Morris, D. C. 2008, PhD thesis, The Pennsylvania State University  
 Morris, D. C., Reeves, J., Palshin, V., et al. 2007, *The Astrophysical Journal*, 654, 413  
 Nousek, J. A., Kouveliotou, C., Grupe, D., et al. 2006, *The Astrophysical Journal*, 642, 389  
 O'Brien, P. T., Willingale, R., Osborne, J. P., et al. 2006, *The Astrophysical Journal*, 647, 1213  
 Piro, L., Amati, L., Antonelli, L., et al. 1998, *Astronomy & Astrophysics*, 331, 41  
 Piro, L., De Pasquale, M., Soffitta, P., et al. 2005, *The Astrophysical Journal*, 623, 314  
 R Core Team. 2013, *R: A Language and Environment for Statistical Computing*  
 Romano, P., Moretti, A., Banat, P. L., et al. 2006, *Astronomy*, 68, 59  
 Roming, P. W. A., Vanden Berk, D. E., Hunsberger, S. D., et al. 2006, *Il Nuovo Cimento B*, 121, 1239  
 Roming, P. W. A., Townsley, L. K., Nousek, J. A., et al. 2000, *Proc. SPIE*, 4140, 76  
 Roming, P. W. A., Hunsberger, S. D., Mason, K. O., et al. 2004, *Proc. SPIE*, 5165, 262  
 Roming, P. W. A., Kennedy, T. E., Mason, K. O., et al. 2005, *Space Science Reviews*, 120, 95  
 Roming, P. W. A., Koch, T. S., Oates, S. R., et al. 2009, *The Astrophysical Journal*, 690, 163  
 Schwarz, G. 1978, *The Annals of Statistics*, 6, 461  
 Swenson, C. A., Roming, P. W. A., De Pasquale, M., & Oates, S. R. 2013, *The Astrophysical Journal*, 774, 2  
 Swenson, C. A., Maxham, A., Roming, P. W. A., et al. 2010, *The Astrophysical Journal*, 718, L14  
 Zeileis, A., Kleiber, C., Kramer, W., & Hornik, K. 2003, *Computational Statistics & Data Analysis*, 44, 109  
 Zeileis, A., Leisch, F., Hornik, K., & Kleiber, C. 2002, *Journal of Statistical Software*, 7, 1  
 Zhang, B., Fan, Y. Z., Dyks, J., et al. 2006, *The Astrophysical Journal*, 642, 354

**Table 1**  
X-ray Flares

Flaring Period	Source Name	$T_{peak}^*$ (s)	$T_{start}$ lower limit* (s)	$T_{stop}$ upper limit* (s)	$\Delta t/t$	Flux Ratio lower limit	Confidence
N	GRB050128	720.13	686.15	784.77	0.14	0.43	0.5163
N	GRB050128	293.30	278.18	305.28	0.09	0.34	0.4182
N	GRB050219A	129.10	126.20	131.46	0.04	0.66	0.7269
N	GRB050219A	262.85	245.68	295.79	0.19	0.72	0.6922
N	GRB050219A	164.02	159.94	169.35	0.06	0.46	0.5689
N	GRB050318	32447.35	28612.78	32788.65	0.13	1.75	0.3661
N	GRB050319	1438.08	1376.84	1510.20	0.09	0.88	0.7775
N	GRB050401	139.69	134.39	151.31	0.12	0.40	0.5326
N	GRB050401	173.49	169.78	187.33	0.10	0.39	0.3651
N	GRB050406	210.50	112.65	354.36	1.15	20.42	0.9250
N	GRB050422	117.30	117.30	243.46	1.08	14.75	0.9557
N	GRB050502B	749.01	136.66	1625.30	1.99	278.87	1.0000
N	GRB050502B	77030.88	24814.44	148657.16	1.61	5.06	1.0000
N	GRB050607	310.98	278.60	686.64	1.31	43.21	1.0000
N	GRB050712	262.74	194.56	414.77	0.84	3.21	1.0000
N	GRB050712	478.89	457.87	546.78	0.19	4.76	1.0000
N	GRB050714B	377.53	310.24	5616.99	14.06	84.09	1.0000
N	GRB050716	388.94	358.61	471.15	0.29	4.97	0.5335
N	GRB050716	174.49	161.11	194.71	0.19	0.29	0.4958
N	GRB050717	98.36	94.31	105.11	0.11	0.18	0.3836
N	GRB050721	232.62	219.54	239.21	0.08	0.26	0.5501
N	GRB050726	277.06	226.61	326.97	0.36	1.73	1.0000
N	GRB050726	163.53	148.62	177.98	0.18	0.42	0.5163
N	GRB050730	430.47	345.56	531.29	0.43	2.87	1.0000
N	GRB050730	677.47	615.53	765.81	0.22	1.23	1.0000
N	GRB050730	224.30	209.24	272.92	0.28	0.95	1.0000
N	GRB050803	726.03	577.64	908.04	0.46	0.55	0.8439
N	GRB050803	1180.30	1003.83	1247.73	0.21	0.72	0.7923
N	GRB050814	2239.74	1077.38	12353.55	5.03	2.63	0.7119
N	GRB050814	262.27	249.64	405.51	0.59	0.46	0.5131
N	GRB050819	16446.42	11135.25	36537.51	1.54	1.88	0.7895
N	GRB050820A	248.09	215.80	4681.53	18.00	59.67	1.0000
N	GRB050822	424.22	336.28	945.97	1.44	40.86	1.0000
N	GRB050822	238.70	208.44	258.12	0.21	2.55	1.0000
N	GRB050822	111075.78	93374.52	150646.78	0.52	2.06	0.4605
N	GRB050908	399.39	294.69	784.93	1.23	14.23	1.0000
N	GRB050908	143.35	129.50	191.89	0.44	1.99	0.9211
N	GRB050915A	105.73	94.78	156.23	0.58	4.91	1.0000
N	GRB050915A	533.32	444.90	658.53	0.40	1.31	0.7139
N	GRB050916	18807.53	17052.58	22517.67	0.29	39.66	1.0000
N	GRB050922B	812.98	615.57	1486.43	1.07	40.08	0.9196
N	GRB050922B	375.96	363.91	391.72	0.07	0.23	0.7037
N	GRB051006	130.83	122.13	144.20	0.17	1.09	0.8349
N	GRB051008	5113.48	4944.48	5250.01	0.06	0.69	0.7256
N	GRB051021B	158.89	126.44	209.28	0.52	360.69	0.6059
N	GRB051117A	1324.39	1257.16	5021.08	2.84	5.60	1.0000
N	GRB051117A	1072.29	819.59	1233.96	0.39	2.33	0.7784
N	GRB051117A	436.58	301.97	751.52	1.03	1.80	0.7747
N	GRB051210	133.23	119.84	156.19	0.27	1.16	0.7904
N	GRB051210	164.01	156.19	217.25	0.37	0.73	0.4352
N	GRB051227	114.33	103.48	165.68	0.54	0.81	1.0000
N	GRB060105	52190.64	40674.94	98642.80	1.11	2.65	0.3072
N	GRB060108	4545.11	4382.39	4703.78	0.07	1.86	0.9791
N	GRB060108	122.79	122.79	337.44	1.75	2.86	0.9784
N	GRB060111A	91.20	82.56	131.18	0.53	1.55	1.0000
N	GRB060111A	168.76	149.80	204.45	0.32	2.63	1.0000
N	GRB060111A	288.18	204.45	525.47	1.11	23.18	1.0000
N	GRB060111A	15916.42	15514.31	16275.01	0.05	1.68	0.4902
N	GRB060111B	156.34	136.70	182.76	0.29	0.48	0.3835
N	GRB060115	399.88	308.46	718.93	1.03	3.57	1.0000
N	GRB060116	179.04	179.04	209.90	0.17	1.34	0.9688
N	GRB060116	1201.25	1089.15	1356.86	0.22	0.86	0.7709
N	GRB060124	571.26	213.78	11441.52	19.65	789.65	1.0000
N	GRB060202	700.75	360.78	1040.55	0.97	5.25	0.9011
N	GRB060204B	121.54	108.08	139.53	0.26	2.74	1.0000
N	GRB060204B	317.43	275.00	493.00	0.69	52.47	1.0000
N	GRB060204B	210.99	198.34	310.00	0.53	2.01	0.5519
N	GRB060206	5446.84	1787.63	23560.91	4.00	3.00	1.0000
N	GRB060210	199.90	164.69	302.20	0.69	12.13	0.8724
N	GRB060210	377.04	302.20	607.66	0.81	7.89	0.8719
N	GRB060210	106.86	104.12	120.23	0.15	0.86	0.5564
N	GRB060218	6473.92	5879.34	10662.93	0.74	1.30	0.5341
N	GRB060223A	1319.42	811.26	5324.44	3.42	13.66	1.0000
N	GRB060223A	387.14	292.65	563.22	0.70	0.97	0.5724

Table 1 — *Continued*

Flaring Period	Source Name	$T_{peak}^*$ (s)	$T_{start}$ lower limit* (s)	$T_{stop}$ upper limit* (s)	$\Delta t/t$	Flux Ratio lower limit	Confidence
Y	GRB060312	109.76	65.74	245.11	1.63	49.66	1.0000
N	GRB060312	542.17	462.80	850.48	0.72	1.79	0.9687
N	GRB060313	191.19	154.84	238.67	0.44	1.90	0.7024
N	GRB060313	137.14	120.54	154.84	0.25	0.79	0.6440
N	GRB060319	280.38	261.55	309.05	0.17	0.77	0.9771
N	GRB060403	73.33	70.07	79.57	0.13	0.94	0.5477
N	GRB060413	642.87	547.94	930.63	0.60	3.37	1.0000
N	GRB060418	130.77	116.61	173.07	0.43	7.22	0.8215
N	GRB060421	6045.43	5177.30	10810.05	0.93	1.28	0.9931
N	GRB060510A	775.42	748.18	807.80	0.08	0.68	0.2755
N	GRB060510A	1201.00	1171.45	1229.73	0.05	0.78	0.2447
Y	GRB060510B	301.22	172.14	468.31	0.98	13.75	1.0000
N	GRB060510B	1005.71	751.94	5502.63	4.72	27.52	0.7393
N	GRB060512	201.90	174.23	379.87	1.02	3.53	1.0000
Y	GRB060526	247.69	181.79	948.01	3.09	389.56	1.0000
N	GRB060602B	195.41	174.52	246.99	0.37	1.19	0.7366
N	GRB060604	136.86	124.30	228.00	0.76	4.86	1.0000
N	GRB060607	98.61	93.41	132.30	0.39	4149.05	1.0000
N	GRB060607	264.86	216.85	389.35	0.65	3542.41	1.0000
N	GRB060607	180.79	169.89	205.33	0.20	1078.69	0.4365
N	GRB060707	186.08	175.41	228.78	0.29	1.41	0.9618
N	GRB060712	299.00	271.43	346.85	0.25	1.70	0.9314
N	GRB060714	137.70	123.58	158.50	0.25	3.76	0.8246
N	GRB060714	175.67	158.50	225.14	0.38	7.44	0.8246
N	GRB060719	200.98	139.27	372.09	1.16	6.68	1.0000
N	GRB060801	109.74	96.11	149.52	0.49	0.64	0.9223
N	GRB060805A	4304.05	579.41	19615.79	4.42	4.97	0.6054
N	GRB060813	515.90	495.86	541.34	0.09	0.72	0.4417
N	GRB060813	109.16	105.35	129.53	0.22	0.42	0.4068
N	GRB060814	130.69	120.75	161.32	0.31	1.18	0.8325
N	GRB060904A	303.95	253.97	454.43	0.66	9.92	1.0000
N	GRB060904A	675.96	634.19	1036.13	0.59	6.89	1.0000
N	GRB060904A	2132.63	1036.13	58529.15	26.96	8.77	0.9432
N	GRB060904A	154.26	162.81	239.88	0.50	-0.14	0.3214
N	GRB060904B	171.72	127.96	3760.36	21.15	243.84	1.0000
N	GRB060906	162.75	162.75	244.43	0.50	4.54	1.0000
N	GRB060908	136.11	131.28	145.01	0.10	1.12	0.9211
N	GRB060919	515.99	353.90	690.68	0.65	0.91	0.9827
N	GRB060926	435.99	391.96	585.62	0.44	0.44	0.6280
N	GRB060929	553.06	371.65	1120.67	1.35	846.44	1.0000
N	GRB061004	70.54	70.54	120.35	0.71	1.15	0.9187
N	GRB061110A	135.58	111.75	209.17	0.72	1.31	1.0000
N	GRB061121	80.53	67.01	100.57	0.42	0.89	0.9752
N	GRB061121	119.28	106.11	128.79	0.19	0.81	0.4126
N	GRB061202	140.58	125.84	184.32	0.42	3.74	1.0000
N	GRB070103	687.45	355.52	907.00	0.80	0.72	0.6708
N	GRB070107	357.16	291.36	399.01	0.30	9.64	1.0000
N	GRB070110	10707.35	4084.37	27535.08	2.19	8.94	1.0000
Y	GRB070129	360.99	230.13	1070.24	2.33	73.58	1.0000
N	GRB070220	107.97	104.71	117.67	0.12	0.68	0.4355
N	GRB070220	523.94	500.25	580.40	0.15	0.68	0.3057
N	GRB070306	181.74	174.80	208.04	0.18	8.01	0.7592
N	GRB070318	270.70	235.64	423.34	0.69	3.06	1.0000
N	GRB070318	193.77	186.64	216.47	0.15	0.50	0.8203
N	GRB070330	222.54	164.56	361.76	0.89	11.87	1.0000
N	GRB070419B	243.76	198.74	325.85	0.52	1.29	0.9989
N	GRB070419B	100.23	86.51	140.86	0.54	0.31	0.2634
N	GRB070420	22932.76	18762.03	23152.81	0.19	8.38	1.0000
N	GRB070518	186.29	96.20	357.02	1.40	14.53	1.0000
N	GRB070520A	235.94	238.83	3975.32	15.84	-0.12	0.5075
N	GRB070520B	187.56	146.20	375.30	1.22	6.66	1.0000
N	GRB070521	331.58	296.68	408.25	0.34	0.74	0.6976
N	GRB070531	427.93	371.50	558.68	0.44	0.99	0.7598
N	GRB070611	3420.85	3420.85	4131.24	0.21	1.23	0.9931
N	GRB070616	485.09	415.16	709.34	0.61	3.25	0.9143
N	GRB070616	757.27	713.97	843.16	0.17	2.03	0.9012
N	GRB070616	198.94	191.33	203.66	0.06	0.90	0.8182
N	GRB070621	145.12	135.99	154.04	0.12	0.96	0.5578
N	GRB070704	303.20	258.01	5209.41	16.33	25.52	1.0000
N	GRB070714A	310.88	234.46	484.19	0.80	1.12	0.7697
N	GRB070714A	904.82	742.63	1369.29	0.69	0.98	0.4904
N	GRB070714B	122.80	114.75	128.57	0.11	0.85	0.2043
N	GRB070721B	311.06	238.98	394.60	0.50	11.79	1.0000
N	GRB070721B	623.00	574.66	748.51	0.28	0.84	0.7423
N	GRB070724A	105.01	89.48	123.46	0.32	1.63	1.0000
N	GRB070802	162.48	162.48	247.07	0.52	2.47	0.9524

Table 1 — *Continued*

Flaring Period	Source Name	$T_{peak}^*$ (s)	$T_{start}$ lower limit* (s)	$T_{stop}$ upper limit* (s)	$\Delta t/t$	Flux Ratio lower limit	Confidence
N	GRB070808	126.53	121.11	144.19	0.18	0.65	0.5954
N	GRB071031	454.98	380.95	6131.18	12.64	5.78	1.0000
N	GRB071031	150.28	141.28	173.11	0.21	0.52	0.8280
N	GRB071031	195.98	187.96	227.76	0.20	0.63	0.7122
N	GRB071031	257.34	244.61	300.07	0.22	1.41	0.6853
N	GRB071104	328810.48	32444.48	33294.06	0.00	-0.23	0.5673
Y	GRB071118	596.12	333.15	1573.09	2.08	11.63	0.7422
N	GRB071122	400.50	357.45	516.66	0.40	0.64	0.6866
N	GRB071227	158.66	153.12	191.64	0.24	0.41	0.7518
Y	GRB080123	166.07	155.98	373.14	1.31	1.26	0.8681
N	GRB080210	189.07	174.65	256.70	0.43	8.61	1.0000
Y	GRB080212	294.14	173.46	448.66	0.94	26.44	1.0000
N	GRB080229A	104.41	93.74	173.11	0.76	0.98	0.9438
Y	GRB080310	205.60	126.20	1131.56	4.89	41.66	1.0000
N	GRB080310	4858.46	1442.36	17540.08	3.31	3.18	0.5355
N	GRB080319B	701334.41	76075.39	2544607.50	3.52	12.28	0.5956
N	GRB080319D	295.75	238.44	490.77	0.85	6.46	0.9597
N	GRB080320	309.90	273.92	444.89	0.55	6.68	1.0000
N	GRB080320	211.29	196.35	273.92	0.37	3.21	0.6243
N	GRB080320	699.37	759.78	972.75	0.30	-0.33	0.6198
N	GRB080325	220.02	198.71	379.57	0.82	2.01	1.0000
N	GRB080325	175.59	163.52	175.59	0.07	-0.10	0.8691
N	GRB080409	441.94	342.75	5615.39	11.93	0.92	0.7722
N	GRB080426	653.06	572.11	736.85	0.25	0.72	0.9387
Y	GRB080506	480.47	366.33	5652.40	11.00	43.69	1.0000
N	GRB080506	174.65	160.37	207.62	0.27	1.07	0.7826
N	GRB080516	463.15	356.73	572.61	0.47	0.89	0.7085
N	GRB080517	131.45	131.45	565.45	3.30	18.58	0.9385
N	GRB080602	906.16	890.47	922.79	0.04	1.53	0.6063
N	GRB080604	972.20	896.44	1065.04	0.17	0.85	0.3884
N	GRB080607	123.97	117.35	209.98	0.75	5.45	1.0000
N	GRB080703	380.77	306.95	420.32	0.30	0.66	0.6119
N	GRB080703	217.34	189.30	306.95	0.54	0.53	0.4867
N	GRB080710	3467.74	3314.73	4716.99	0.40	0.58	0.5107
N	GRB080714	165.06	143.53	170.17	0.16	1.30	0.4506
N	GRB080723A	160.30	133.13	193.33	0.38	0.69	0.9053
N	GRB080727A	317.82	243.40	426.37	0.58	0.93	0.9880
N	GRB080802	94.21	86.43	104.05	0.19	2.80	1.0000
N	GRB080804	117.49	114.24	121.16	0.06	0.50	0.7253
N	GRB080804	137.47	133.67	145.29	0.08	0.33	0.5335
Y	GRB080805	120.25	89.90	224.96	1.12	4.70	1.0000
N	GRB080810	103.46	88.29	132.09	0.42	4.54	1.0000
Y	GRB080810	208.00	187.38	335.21	0.71	5.38	1.0000
N	GRB080905A	256.22	200.92	310.51	0.43	0.81	0.7808
N	GRB080906	180.59	160.85	257.76	0.54	2.17	1.0000
N	GRB080906	577.76	552.98	709.40	0.27	1.07	0.8932
N	GRB080913	1863.81	984.59	8580.70	4.08	6.46	0.9997
N	GRB080913	485.17	305.21	608.29	0.62	1.24	0.7351
N	GRB080916A	92.22	91.42	97.82	0.07	0.74	0.7920
N	GRB080919	285.07	206.63	711.80	1.77	5.82	0.9984
N	GRB080928	206.76	176.27	269.13	0.45	3.94	1.0000
N	GRB080928	349.63	343.42	400.61	0.16	2.07	1.0000
N	GRB081008	301.44	284.17	403.08	0.39	5.90	1.0000
Y	GRB081008	171.82	126.22	237.45	0.65	2.05	0.7415
N	GRB081011	113.45	113.45	208.35	0.84	5.85	1.0000
N	GRB081011	52704.36	44311.60	72949.15	0.54	1.03	0.6849
N	GRB081024A	168.52	129.46	254.25	0.74	13.52	0.9330
N	GRB081102	954.84	876.46	5796.52	5.15	30.54	1.0000
N	GRB081121	3645.38	3442.15	3913.02	0.13	0.97	0.5174
N	GRB081128	32368.08	14915.69	72762.53	1.79	1.80	0.4221
Y	GRB081210	141.11	111.54	249.65	0.98	8.48	1.0000
N	GRB081210	316.95	282.45	471.49	0.60	1.78	0.8943
N	GRB090111	474.40	174.38	1201.42	2.16	20.85	1.0000
N	GRB090123	1781.95	1452.29	1912.69	0.26	1.15	0.7904
N	GRB090123	483.95	416.29	667.62	0.52	1.35	0.4320
N	GRB090309	4741.20	4352.06	16512.02	2.56	0.89	0.6757
N	GRB090328A	93405.55	63169.38	98447.09	0.38	1.24	0.5401
Y	GRB090407	134.67	111.10	746.38	4.72	12.41	1.0000
N	GRB090417B	1507.40	1244.48	5401.39	2.76	11.91	1.0000
N	GRB090418A	157.92	152.74	172.02	0.12	0.31	0.3574
Y	GRB090419	321.96	265.96	1015.39	2.33	4.18	0.9837
N	GRB090422	96.73	73.85	120.62	0.48	0.82	0.9881
N	GRB090423	174.42	136.90	273.99	0.79	13.22	1.0000
N	GRB090426	296.20	200.23	417.24	0.73	0.60	0.6446
N	GRB090429A	169.05	156.27	209.16	0.31	2.77	0.9287
N	GRB090429A	101.24	88.71	117.80	0.29	0.84	0.7504

Table 1 — *Continued*

Flaring Period	Source Name	$T_{peak}^*$ (s)	$T_{start}$ lower limit* (s)	$T_{stop}$ upper limit* (s)	$\Delta t/t$	Flux Ratio lower limit	Confidence
N	GRB090429A	130.17	120.73	138.18	0.13	0.75	0.6688
N	GRB090429A	252.31	241.35	37669.76	148.34	1.23	0.5717
N	GRB090429B	626.04	290.50	15542.75	24.36	3.86	0.9746
N	GRB090515	159.26	79.51	288.97	1.32	16.00	1.0000
N	GRB090515	204.58	201.16	207.78	0.03	11386341.84	0.2487
N	GRB090516	274.00	267.27	282.37	0.06	5.95	1.0000
N	GRB090519	221.48	203.87	242.48	0.17	1.27	0.8710
N	GRB090529	13785.24	27785.00	148937.11	8.79	0.21	0.8682
N	GRB090530	263.97	192.74	303.82	0.42	0.71	0.8561
N	GRB090607	119.71	96.30	549.87	3.79	7.91	1.0000
N	GRB090621A	268.16	153.69	795.78	2.39	552.54	1.0000
N	GRB090628	14599.13	3522.28	42257.78	2.65	4.21	0.7659
N	GRB090709A	88.71	79.38	105.82	0.30	3.10	1.0000
N	GRB090709A	399.78	366.96	466.43	0.25	0.91	0.8495
N	GRB090709A	281.83	248.49	307.03	0.21	0.65	0.6830
Y	GRB090715B	289.92	59.33	363.63	1.05	30.31	1.0000
N	GRB090727	269.62	131.63	4078.65	14.64	109.21	1.0000
N	GRB090727	171920.17	113699.93	285295.30	1.00	1.43	0.6279
N	GRB090728	227.44	194.06	315.61	0.53	0.80	0.4978
N	GRB090809	178.61	170.45	3512.68	18.71	15.04	1.0000
N	GRB090809	4702.60	3628.26	9240.61	1.19	8.73	1.0000
N	GRB090809	22799.20	11459.20	31007.17	0.86	1.05	0.6837
N	GRB090812	137.77	102.78	199.20	0.70	0.66	0.9197
N	GRB090812	257.63	246.38	318.82	0.28	1.78	0.8979
N	GRB090831C	182.28	155.56	296.96	0.78	7.05	0.9134
N	GRB090831C	431.80	371.25	617.50	0.57	2.38	0.7988
N	GRB090902B	436259.21	338770.66	703452.43	0.84	1.32	0.5544
N	GRB090904A	300.01	288.54	358.19	0.23	2.76	0.9685
N	GRB090904A	6758.74	6107.89	10532.16	0.65	0.93	0.3939
N	GRB090904B	120.51	120.51	145.20	0.20	3.38	0.9745
N	GRB090904B	903.80	803.70	967.61	0.18	1.00	0.5399
N	GRB090912	781.36	781.36	850.68	0.09	2.26	0.8477
N	GRB090926A	46846.73	46677.98	51695.21	0.11	0.78	0.5713
N	GRB090926A	203029.11	193054.42	232375.73	0.19	0.89	0.3281
N	GRB090926A	86116.04	81266.45	144410.24	0.73	1.71	0.2109
N	GRB090927	2229.09	2229.09	2649.06	0.19	0.87	0.9198
Y	GRB090929B	149.58	81.59	3453.39	22.54	13.26	1.0000
N	GRB091024	5145.00	4606.70	32019.65	5.33	1.63	0.9204
N	GRB091024	3207.78	3207.78	3395.99	0.06	1.92	0.7846
N	GRB091026	341.14	288.89	545.75	0.75	6.52	0.9932
N	GRB091026	877.11	618.25	5557.31	5.63	3.06	0.7291
N	GRB091026	173.04	158.18	222.06	0.37	1.20	0.5386
N	GRB091029	323.60	233.28	601.56	1.14	8.67	0.8354
N	GRB091104	203.85	191.11	250.03	0.29	1.52	0.8765
N	GRB091109A	248.34	227.27	278.06	0.20	0.71	0.6050
N	GRB091130B	99.92	83.85	171.67	0.88	3.15	0.9167
N	GRB091208B	101.40	101.40	144.38	0.42	0.93	0.8409
N	GRB091221	106.33	87.64	196.18	1.02	10.91	0.7838
N	GRB091221	62.99	62.99	87.64	0.39	5.96	0.7721
N	GRB100111A	951.32	817.28	4644.77	4.02	0.80	0.9311
N	GRB100117A	181.60	150.75	470.16	1.76	2.35	0.7065
Y	GRB100212A	120.43	64.70	459.25	3.28	21.32	1.0000
N	GRB100212A	668.35	610.33	795.63	0.28	12.29	0.7407
N	GRB100219A	17800.44	13234.12	18999.62	0.32	0.98	0.7968
Y	GRB100302A	250.31	225.14	780.53	2.22	13.32	1.0000
N	GRB100302A	134.48	123.44	150.19	0.20	1.51	0.8935
N	GRB100302A	188.31	174.49	201.33	0.14	1.40	0.7201
N	GRB100316B	1064.41	395.16	37185.71	34.56	2.82	0.9665
N	GRB100316C	261.01	188.34	574.54	1.48	1.14	0.9899
N	GRB100413A	149.91	138.19	160.53	0.15	0.90	0.7837
N	GRB100413A	278.44	250.86	289.21	0.14	1.05	0.7793
N	GRB100413A	222.48	192.98	234.85	0.19	0.83	0.5932
N	GRB100425A	70.97	69.85	85.61	0.22	2.54	0.8257
N	GRB100425A	482.86	347.57	610.09	0.54	0.95	0.5149
N	GRB100504A	52.96	52.96	69.43	0.31	10.39	1.0000
N	GRB100504A	81.58	74.95	117.28	0.52	1.02	0.8652
N	GRB100513A	213.64	163.43	698.32	2.50	5.83	0.9078
N	GRB100522A	2021.97	1703.73	5996.03	2.12	0.46	0.4785
N	GRB100526A	183.95	168.61	259.30	0.49	1.80	0.9893
N	GRB100614A	161.92	154.70	180.64	0.16	0.63	0.9164
N	GRB100614A	957.82	898.59	1163.40	0.28	0.76	0.5811
N	GRB100619A	941.53	862.01	5001.70	4.40	71.41	1.0000
N	GRB100619A	88.37	72.86	123.36	0.57	6.76	0.9822
N	GRB100621A	65.92	65.92	69.85	0.06	3.53	0.9805
N	GRB100625A	191.48	134.47	326.50	1.00	0.69	0.5371
N	GRB100702A	361.05	237.42	442.05	0.57	1.19	0.3849



Table 1 — *Continued*

Flaring Period	Source Name	$T_{peak}^*$ (s)	$T_{start}$ lower limit* (s)	$T_{stop}$ upper limit* (s)	$\Delta t/t$	Flux Ratio lower limit	Confidence
Y	GRB100704A	173.54	145.30	348.81	1.17	16.89	0.9734
N	GRB100725A	69.18	69.18	73.55	0.06	2.04	0.7670
Y	GRB100725B	217.54	114.22	369.85	1.18	56.43	0.7892
N	GRB100727A	243.37	163.06	669.58	2.08	63.09	1.0000
N	GRB100728A	574.10	512.64	654.75	0.25	6.75	0.8812
N	GRB100728A	317.33	298.03	380.33	0.26	4.43	0.8121
N	GRB100728A	701.40	673.31	886.50	0.30	2.50	0.7756
N	GRB100728A	123.41	109.40	137.56	0.23	0.93	0.7111
N	GRB100728A	392.83	380.33	415.01	0.09	3.55	0.5152
N	GRB100728A	221.84	197.98	247.34	0.22	1.01	0.5001
N	GRB100728A	88.39	82.89	100.06	0.19	0.48	0.3698
N	GRB100728A	462.31	448.44	498.57	0.11	1.14	0.2746
N	GRB100728A	269.42	251.77	292.42	0.15	0.88	0.2122
N	GRB100728B	104.13	88.37	144.33	0.54	0.65	0.6330
N	GRB100802A	478.02	274.48	4633.13	9.12	47.29	1.0000
N	GRB100802A	33392.37	29132.41	40373.93	0.34	1.55	0.4487
N	GRB100805A	636.29	423.70	4348.88	6.17	23.06	1.0000
N	GRB100807A	88.35	77.18	262.37	2.10	27.40	1.0000
N	GRB100814A	147.00	119.46	357.38	1.62	2.18	0.9918
N	GRB100814A	139311.60	69791.07	374420.00	2.19	1.81	0.6527
N	GRB100816A	73.82	73.82	91.72	0.24	1.05	0.8600
N	GRB100816A	139.65	125.09	211.06	0.62	1.24	0.8562
N	GRB100823A	4748.51	4398.85	5317.38	0.19	2.07	0.4737
Y	GRB100901A	399.18	132.52	3851.99	9.32	42.59	1.0000
N	GRB100901A	28505.81	12080.08	67586.83	1.95	1.68	0.8896
N	GRB100902A	411.02	355.83	634.69	0.68	131.92	1.0000
N	GRB100902A	2015.83	1846.22	2194.78	0.17	1.09	0.5733
Y	GRB100905A	319.46	161.44	563.72	1.26	47.64	1.0000
N	GRB100905A	5412.16	1850.27	7200.81	0.99	1.13	0.5858
N	GRB100905A	1683.70	1535.22	1850.70	0.19	0.95	0.4221
N	GRB100906A	117.90	86.15	199.41	0.96	23.16	1.0000
N	GRB100915A	157.84	153.95	166.30	0.08	0.34	0.6480
N	GRB100915A	191.01	179.20	194.34	0.08	0.78	0.3489
N	GRB101011A	120.10	108.08	143.44	0.29	0.65	0.6533
N	GRB101011A	241.37	215.77	296.95	0.34	0.98	0.4961
N	GRB101017A	849.85	679.06	1058.20	0.45	0.60	0.5488
N	GRB101017A	181.22	173.93	193.02	0.11	0.71	0.3320
N	GRB101023A	75.25	75.25	77.63	0.03	8.14	0.9456
N	GRB101024A	513.90	482.84	576.60	0.18	0.33	0.3508
N	GRB101030A	86.68	84.33	89.96	0.06	0.26	0.4242
N	GRB101117B	184.22	161.53	244.90	0.45	0.44	0.6498
N	GRB101117B	266.06	244.90	312.12	0.25	0.80	0.5989
N	GRB101204A	316164.03	290600.72	334743.34	0.14	0.88	0.3346
N	GRB101213A	95.34	95.34	98.27	0.03	0.45	0.5303
N	GRB101213A	63343.55	34883.14	80229.22	0.72	1.36	0.5222
N	GRB101219A	170.16	84.25	270.53	1.09	7.92	0.9501
N	GRB101219B	327.66	300.05	554.06	0.78	0.94	0.6871
N	GRB101225A	22590.84	10740.74	56608.60	2.03	34.28	0.8784
N	GRB101225A	6108.55	4988.46	7477.77	0.41	5.03	0.7767
Y	GRB110102A	263.18	193.02	443.52	0.95	38.17	1.0000
N	GRB110102A	139.57	139.57	178.35	0.28	16.64	1.0000
N	GRB110106B	829.59	583.60	1111.41	0.64	0.62	0.7593
N	GRB110112A	752.34	601.82	4917.12	5.74	0.89	0.9922
N	GRB110112A	268.00	186.65	447.82	0.97	0.65	0.8104
N	GRB110119A	197.09	164.64	305.24	0.71	0.11	0.9121
N	GRB110119A	48.53	48.53	68.56	0.41	1.69	0.8997
N	GRB110119A	127.42	99.59	147.52	0.38	2.03	0.8311
N	GRB110119A	657.91	533.00	4942.73	6.70	6.81	0.7989
N	GRB110119A	385.41	364.54	441.68	0.20	2.36	0.5654
N	GRB110128A	129.73	129.73	315.19	1.43	2.02	0.9991
N	GRB110128A	171625.12	83377.92	217445.33	0.78	1.12	0.5554
N	GRB110201A	148.34	110.01	308.08	1.34	2.19	0.7542
N	GRB110205A	615.56	595.33	716.93	0.20	1.99	0.8407
N	GRB110205A	82840.56	76124.31	118778.54	0.51	0.81	0.2399
N	GRB110208A	68.62	68.62	143.90	1.10	2.96	0.9999
N	GRB110208A	844.81	617.34	5677.35	5.99	0.71	0.7111
N	GRB110213A	98.78	87.04	103.59	0.17	0.75	0.4149
N	GRB110223A	275.06	188.23	353.46	0.60	0.80	0.7730
N	GRB110223B	65.15	58.32	77.63	0.30	1.72	0.8741
N	GRB110223B	1173.23	1075.00	1235.58	0.14	1.18	0.6455
N	GRB110305A	358.97	253.95	638.55	1.07	1.05	0.5774
N	GRB110312A	154.00	148.94	168.46	0.13	1.13	0.9126
N	GRB110312A	423.56	322.33	529.20	0.49	0.77	0.7002
N	GRB110312A	737.88	646.25	808.11	0.22	0.53	0.3664
N	GRB110312A	216773.86	141370.86	363358.27	1.02	0.92	0.2426
N	GRB110315A	514.75	411.47	3796.30	6.58	8.86	0.9969

Table 1 — *Continued*

Flaring Period	Source Name	$T_{peak}^*$ (s)	$T_{start}$ lower limit* (s)	$T_{stop}$ upper limit* (s)	$\Delta t/t$	Flux Ratio lower limit	Confidence
N	GRB110318B	140.05	110.67	275.63	1.18	1.98	0.9708
N	GRB110319A	65.96	62.89	67.85	0.08	0.37	0.3692
N	GRB110407A	436.34	401.55	802.43	0.92	-0.29	1.0000
N	GRB110407A	4967.67	4448.41	5294.80	0.17	-0.66	0.4489
N	GRB110414A	385.10	275.54	648.81	0.97	7.05	0.8878
N	GRB110414A	155.69	139.68	172.83	0.21	0.80	0.6283
N	GRB110520A	258.16	146.39	494.65	1.35	6.61	0.9241
N	GRB110520A	625.88	494.65	737.50	0.39	0.96	0.7595
N	GRB110521A	184.23	215.74	524.90	1.68	0.43	0.7281
N	GRB110530A	7344.57	2560.24	13542.38	1.50	0.57	0.7548
N	GRB110530A	1341.81	1009.04	1718.77	0.53	1.25	0.6712
N	GRB110610A	217.98	179.12	291.11	0.51	1.11	0.7112
N	GRB110610A	653.14	614.80	811.51	0.30	1.83	0.6782
N	GRB110610A	199925.99	119058.16	298760.95	0.90	1.34	0.6189
N	GRB110625A	726.77	685.98	829.53	0.20	0.77	0.4342
N	GRB110709A	56.12	56.12	75.16	0.34	1.66	1.0000
N	GRB110709A	91.55	87.76	109.09	0.23	0.96	0.6242
Y	GRB110709B	650.15	417.88	1522.12	1.70	37.91	1.0000
N	GRB110709B	70.72	70.72	112.03	0.58	4.06	0.7481
N	GRB110709B	157.67	133.39	256.11	0.78	0.76	0.7203
N	GRB110715A	50165.92	35049.31	257277.36	4.43	2.92	0.5119
N	GRB110726A	398.09	354.92	492.30	0.35	1.16	0.9631
N	GRB110726A	52.74	48.97	117.52	1.30	0.42	0.9532
N	GRB110801A	382.04	322.01	774.21	1.18	77.04	1.0000
N	GRB110801A	213.18	176.15	261.79	0.40	2.21	0.6649
N	GRB110820A	269.30	142.11	558.35	1.55	1072.55	1.0000
N	GRB110915A	161.67	148.71	216.96	0.42	1.41	0.7723
N	GRB110921A	224.20	155.43	403.30	1.11	3.71	0.7655
N	GRB110921A	526.15	403.30	830.05	0.81	5.92	0.6207
N	GRB110921A	1285.70	1182.23	1346.57	0.13	0.93	0.3762
Y	GRB111016A	610.62	387.58	4950.64	7.47	119.78	1.0000
N	GRB111018A	118.30	118.30	191.88	0.62	7.10	0.9997
N	GRB111020A	904.74	557.83	1204.88	0.72	1.05	0.6795
N	GRB111020A	34831.61	25977.80	52426.19	0.76	1.22	0.5243
N	GRB111022B	455.80	410.88	521.26	0.24	0.63	0.5284
Y	GRB111103B	115.88	110.88	4672.68	39.37	30.10	1.0000
N	GRB111107A	332.37	91.67	587.32	1.49	6.95	0.6913
N	GRB111117A	150.16	107.95	247.29	0.93	0.59	0.7561
N	GRB111123A	487.90	466.14	656.27	0.39	1.91	0.9799
N	GRB111123A	285.37	267.58	300.85	0.12	0.50	0.5189
N	GRB111123A	146.21	139.44	157.62	0.12	0.34	0.4287
N	GRB111129A	254.03	194.19	357.28	0.64	0.56	0.6207
N	GRB120102A	1074.69	937.13	10435.95	8.84	13.79	0.9622
N	GRB120121A	108.03	357.28	154.60	-1.88	4.91	0.9966
N	GRB120121A	1451.90	928.72	6499.65	3.84	0.96	0.5121
N	GRB120213A	5511.00	957.62	11236.18	1.87	2.52	0.8825
N	GRB120224A	99.14	99.14	194.32	0.96	30.91	0.9996
N	GRB120224A	1116.54	582.13	5248.08	4.18	1.94	0.8922
N	GRB120305A	117.96	86.36	310.19	1.90	2.15	0.9957
Y	GRB120308A	123.68	111.40	316.02	1.65	6.91	1.0000
N	GRB120308A	2386.69	1932.85	5891.78	1.66	0.63	0.4988
N	GRB120311A	66716.90	33092.84	104785.26	1.07	0.89	0.9656
N	GRB120312A	90.91	90.91	132.31	0.46	2.01	0.9973
N	GRB120320A	161.22	161.22	312.33	0.94	52.97	0.9995
N	GRB120320A	41696.11	16636.81	139911.52	2.96	3.10	0.5723
N	GRB120324A	102.84	99.97	120.89	0.20	1.09	0.8069
N	GRB120324A	40264.89	17496.23	68368.09	1.26	-0.24	0.7154
N	GRB120327A	931.16	856.83	963.57	0.11	0.79	0.3666
N	GRB120328A	63.45	63.45	88.04	0.39	3.62	0.9258
N	GRB120328A	123.19	88.04	232.50	1.17	9.99	0.9121
N	GRB120328A	551.99	366.34	783.08	0.75	1.67	0.6212
N	GRB120401A	239.16	196.14	350.84	0.65	0.82	0.6788
N	GRB120401A	105.55	105.55	107.95	0.02	0.78	0.4007
N	GRB120514A	142.80	126.64	471.16	2.41	13.47	0.9998
N	GRB120514A	643.81	471.16	4497.94	6.25	7.07	0.6668
N	GRB120521A	216.64	98.67	325.92	1.05	1.77	0.9789
N	GRB120521B	6380.21	5604.57	7181.97	0.25	1.81	0.3365
N	GRB120612A	4956.31	1337.61	17301.26	3.22	8.38	0.9224
N	GRB120612A	181.49	171.17	193.16	0.12	1.57	0.5148
N	GRB120701A	305.16	273.31	459.20	0.61	1.21	0.8231
N	GRB120701A	634.48	538.54	6076.92	8.73	0.83	0.5857
N	GRB120703A	72.54	72.54	92.46	0.27	1.70	0.9290
N	GRB120703A	177.49	159.99	193.41	0.19	0.84	0.6880
N	GRB120703A	232.24	214.10	252.48	0.17	0.84	0.3913
N	GRB120711B	805.15	443.94	892.78	0.56	2.78	0.9424
N	GRB120711B	357.80	341.53	417.47	0.21	0.93	0.6084

Table 1 — *Continued*

Flaring Period	Source Name	$T_{peak}^*$ (s)	$T_{start}$ lower limit* (s)	$T_{stop}$ upper limit* (s)	$\Delta t/t$	Flux Ratio lower limit	Confidence
N	GRB120712A	126970.53	67633.74	462512.44	3.11	2.60	0.7872
N	GRB120714A	29832.97	21938.09	42777.41	0.70	0.59	0.3589
N	GRB120722A	300.58	217.42	558.65	1.14	3.59	0.8054
N	GRB120722A	141.60	141.60	217.42	0.54	6.66	0.7907
N	GRB120724A	119.95	117.16	129.34	0.10	0.43	0.5839
N	GRB120728A	136.62	136.62	236.80	0.73	15.00	0.9962
N	GRB120728A	548.01	357.73	1061.73	1.28	18.40	0.8091
N	GRB120729A	513.22	442.45	565.39	0.24	0.52	0.5557
N	GRB120729A	95.58	90.39	97.60	0.08	0.68	0.5227
N	GRB120804A	82.82	82.82	104.29	0.26	1.13	0.9142
N	GRB120804A	289.82	260.75	418.23	0.54	0.86	0.6700
N	GRB120807A	115.47	101.13	221.15	1.04	6.93	0.9920
N	GRB120816A	210.72	172.29	257.86	0.41	0.89	0.6112
N	GRB120816A	497.47	383.06	580.38	0.40	0.87	0.3832
N	GRB120907A	175.19	121.88	311.06	1.08	0.48	0.6776
N	GRB120911A	4752.70	4548.38	5063.46	0.11	1.10	0.7967
N	GRB120922A	324.66	305.30	349.92	0.14	1.56	0.5833
N	GRB120922A	411.67	361.28	490.65	0.31	3.35	0.2708
N	GRB121001A	373.95	335.69	421.89	0.23	0.81	0.4449
N	GRB121011A	4044.76	3792.69	4241.53	0.11	1.42	0.3371
N	GRB121011A	4505.02	4241.53	4747.37	0.11	1.48	0.3131
N	GRB121024A	205.13	182.87	247.53	0.32	0.31	0.9336
N	GRB121024A	277.11	247.53	352.16	0.38	2.08	0.6950
N	GRB121027A	6074.90	1150.72	35420.68	5.64	442.82	0.9853
N	GRB121027A	247.49	221.07	521.32	1.21	3.40	0.8134
N	GRB121028A	765.23	620.09	1257.88	0.83	9.71	0.8283
N	GRB121102A	56.96	54.23	61.32	0.12	0.51	0.7088
N	GRB121108A	139.66	104.34	503.56	2.86	113.53	1.0000
N	GRB121108A	623.81	751.62	823.91	0.12	-0.20	0.4341
N	GRB121117A	83.17	76.32	104.76	0.34	0.40	0.5248
N	GRB121123A	244.22	190.70	917.74	2.98	18.76	1.0000
N	GRB121125A	91.89	88.06	122.54	0.38	1.60	0.9352
N	GRB121128A	91.35	88.11	127.72	0.43	0.67	0.8100
N	GRB121209A	80.29	80.29	133.72	0.67	8.88	0.9983
N	GRB121211A	175.84	124.51	294.51	0.97	9.78	1.0000
N	GRB121211A	96.63	85.88	105.46	0.20	1.25	0.5686
N	GRB121212A	221.09	131.29	494.36	1.64	16.57	0.9999
N	GRB121212A	577.29	494.36	939.07	0.77	17.14	0.8500
N	GRB121212A	58.48	58.48	131.29	1.25	3.96	0.6032
N	GRB121217A	736.16	222.19	1625.91	1.91	165.87	1.0000
N	GRB121226A	197.74	140.95	275.39	0.68	1.30	0.8769
N	GRB121229A	458.62	344.76	5173.39	10.53	35.27	1.0000
N	GRB121229A	232.48	216.72	261.15	0.19	0.51	0.4989

**Note.** — Flares are listed in chronological order by GRB date, then sorted by confidence. \*All times are relative to the time of the initial burst trigger.  $\Delta t/t$  is calculated as  $(T_{stop} - T_{start})/T_{peak}$ .  $T_{start}$  and  $T_{stop}$  are lower and upper limits, respectively. Flux Ratio is calculated as the flux at the flare peak time divided by the extrapolated flux of the underlying light curve at the same time, normalized using the flux of the underlying light curve, and is a lower limit of the actual peak flux ratio. The confidence measure represents the fraction of times the flare was identified during the 10,000 Monte Carlo simulations. The first column identifies whether the identified feature comes from an overlapping ‘fairing period’.

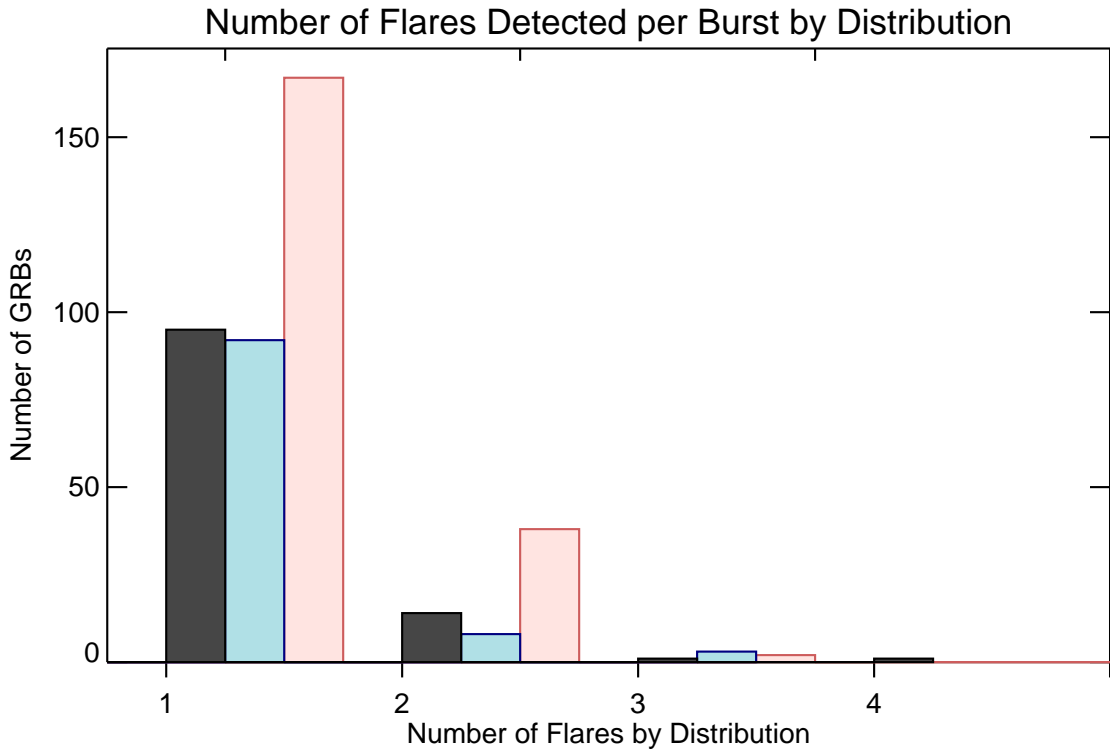


**Figure 1.** Histogram of the number of detected flares per GRB by group. The three distributions are the gold (black font), silver (blue font) and bronze (red font) groups described in the text.

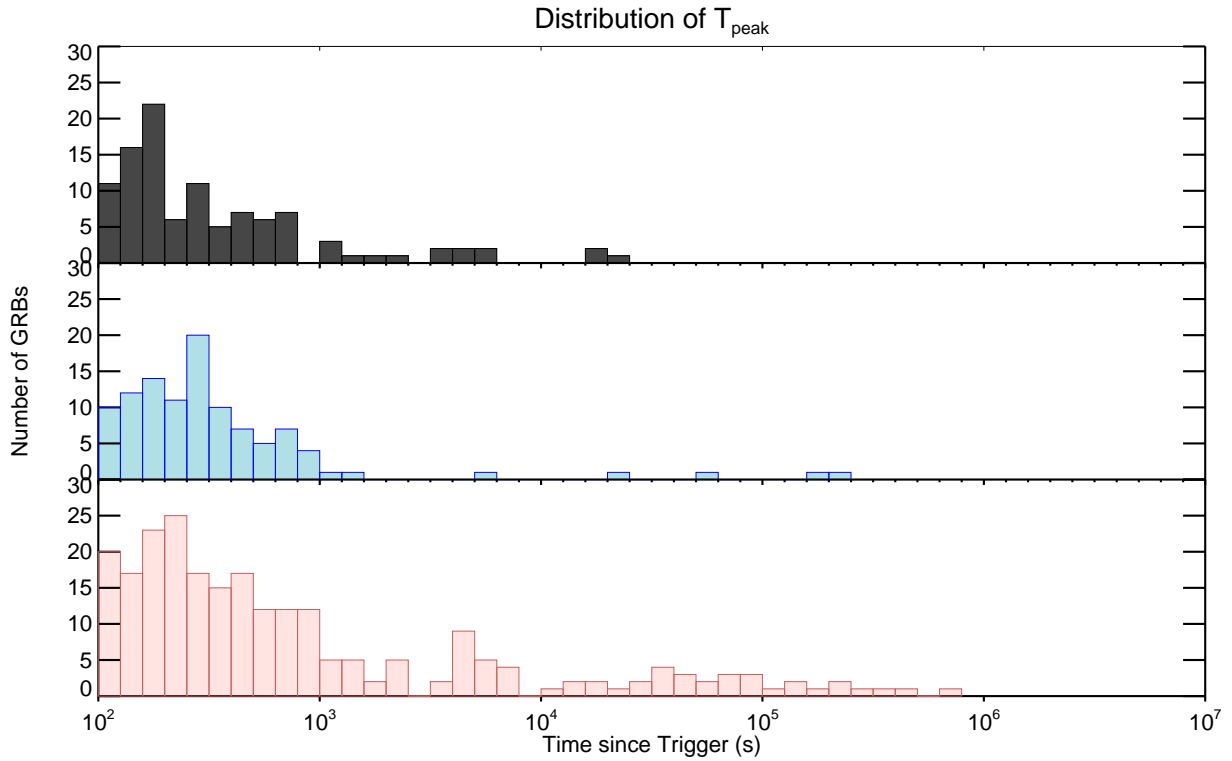


**Figure 2.** Histogram of the distribution of  $T_{peak}$ . The three distributions are the gold (top), silver (middle) and bronze (bottom) distributions described in the text.

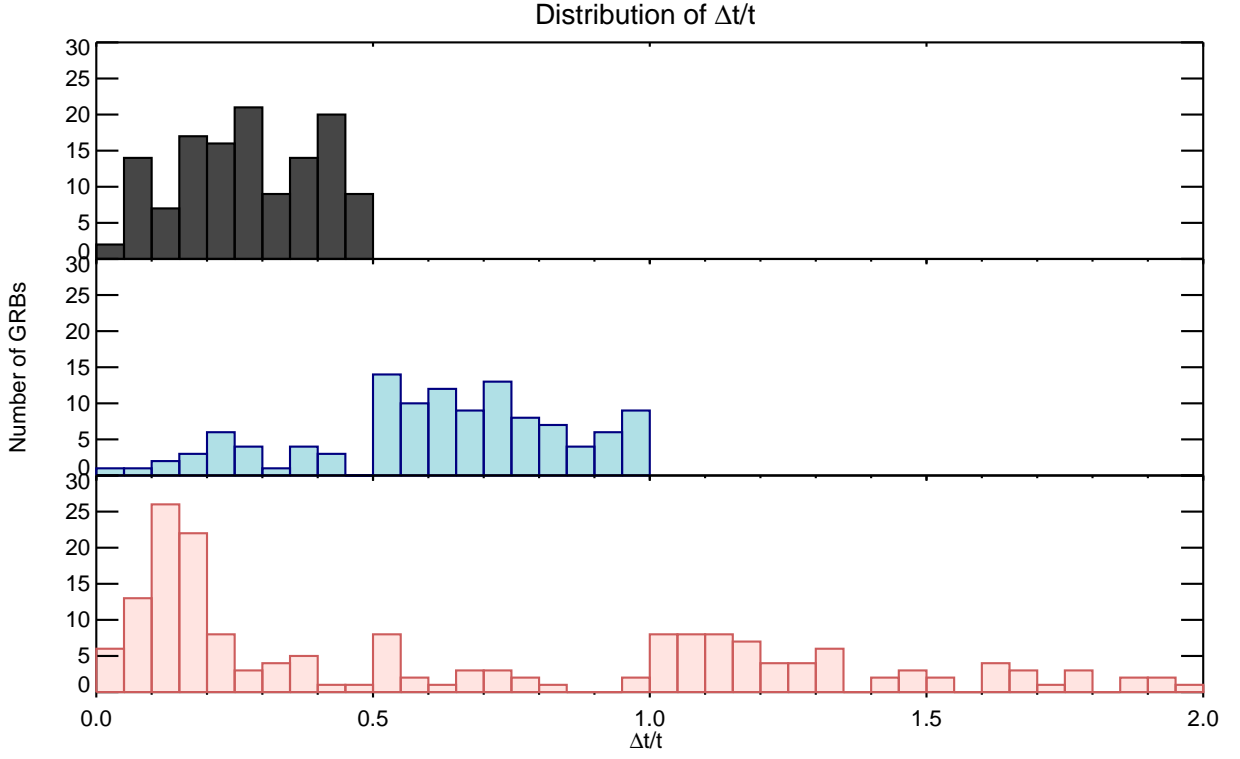


**Figure 3.** Distribution of  $\Delta t/t$ , calculated as  $(T_{stop} - T_{start})/T_{peak}$ , for the detected flares. The three flares with  $\Delta t/t > 2.0$  are omitted for scaling purposes. The three distributions are the gold (top), silver (middle) and bronze (bottom) distributions described in the text.

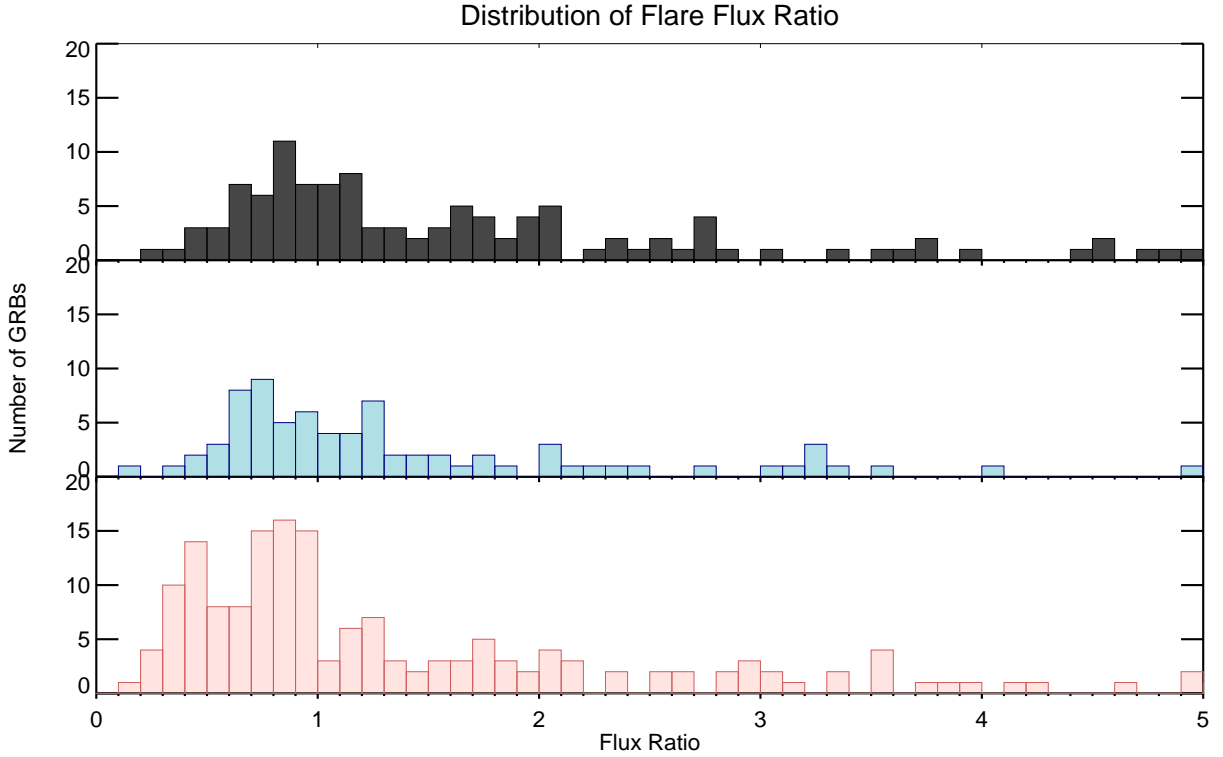


**Figure 4.** Distribution of flare flux ratio, relative to the underlying light curve. The flares with flux ratios  $> 5$  are omitted for scaling purposes. The three distributions are the gold (top), silver (middle) and bronze (bottom) distributions described in the text.